ACS APPLIED MATERIALS & INTERFACES

Functional Inorganic Materials and Devices

Screening and Design of Novel 2D Ferromagnetic Materials with High Curie Temperature above Room Temperature

Zhou Jiang, Peng Wang, Jianpei Xing, Xue Jiang, and Jijun Zhao

ACS Appl. Mater. Interfaces, **Just Accepted Manuscript** • DOI: 10.1021/acsami.8b14037 • Publication Date (Web): 23 Oct 2018

Just Accepted

ACS Publications

is published by the American Chemical Society. 1155 Sixteenth Street N.W., Washington, DC 20036

Screening and Design of Novel 2D Ferromagnetic Materials with High Curie Temperature above Room Temperature

*Zhou Jiang, Peng Wang, Jianpei Xing, Xue Jiang * and Jijun Zhao**

Key Laboratory of Material Modification by Laser, Ion and Electron Beams (Dalian University of Technology), Ministry of Education, Dalian, 116024, China

* Corresponding authors: jiangx@dlut.edu.cn (Xue Jiang), zhaojj@dlut.edu.cn (Jijun Zhao)

ABSTRACT

Two-dimensional (2D) intrinsic ferromagnets with high Curie temperature (T_C) are desirable for spintronic applications. Using systematical first-principles calculations, we investigate the electronic and magnetic properties of 22 monolayer 2D materials with layered bulk phases. From these candidates, we screen out five ferromagnetic monolayer materials belonging to three types of structures: type *i* (ScCl, YCl, LaCl), type *ii* ($LaBr_2$), and type *iii* (CrSBr). Type *i* is a kind of metallic ferromagnetic materials, while $LaBr_2$ and CrSBr of type *ii* and *iii* are small-bandgap ferromagnetic semiconductors with T_C near room temperature. Moreover, ferromagnetic CrSBr monolayer possesses a large magnetic moment of ~3 μ_B per Cr atom originated from its distorted octahedron coordination. The robust ferromagnetism of CrSBr monolayer is ascribed to the halogen-mediated (Cr-Br-Cr) and chalcogen-mediated (Cr-S-Cr) superexchange interactions, then an isoelectronic substitution strategy is proposed to tailor the magnetic coupling strength. Hence, monolayer structures of CrSI, CrSCl, CrSeBr with notably enhanced Curie temperature up to 500 K as well as favorable formation energy are designed. The moderate interlayer binding energy and high T_C make these monolayer ferromagnetic materials feasible for experimental synthesis and attractive as 2D spintronic devices.

KEYWORDS: ferromagnetic materials, two-dimensional materials, Curie temperature, superexchange interaction, crystal field, isoelectronic substitution

1. INTRODUCTION

Two-dimensional (2D) ferromagnetic materials are essential for the next-generation spintronic devices.[1-3] For practical device applications, the 2D ferromagnets require high Curie temperature (T_C) above room temperature. Thus, extensive theoretical efforts have been devoted to predicting intrinsic 2D ferromagnetic monolayer materials with relatively high T_C, including transition metal halogenides MX_3/MX_2,[4-5] ternary transition metal compounds (ABX_3),[6-7] transition metal dischalcogenides (TMD),[8-9] transition metal carbide/nitrides (MXene or TMN_2),[10-13] transition metal borides (MBene),[14] and 2D metal-organic frameworks (MOF).[15-17]

Despite the large variety of potential 2D ferromagnets from theoretical predictions, it is rather difficult to fabricate these ultrathin 2D ferromagnets in laboratory. Experimentalists have already explored several possible 2D ferromagnetic sheets with thickness down to a few nanometers, including Co_9Se_8 (thickness ~0.52 nm), VSe_2 nanosheets (thickness 2.28~4.65 nm), α-Fe_2O_3 (half-unit-cell), and thin flakes of $Cr_2Ge_2Te_6$.[18-21] However, 2D materials reaching the monolayer limit with long-range magnetic order are rarely observed in laboratory. In 2017, Xu's[22] and Zhang's[23] groups simultaneously reported the first two examples of atomically thin ferromagnetic materials, i.e., monolayer CrI_3 and bilayer $Cr_2Ge_2Te_6$. However, the measured Curie temperatures for CrI_3 (T_C = 45 K) and $Cr_2Ge_2Te_6$ (T_C = 20 K) are far below room temperature. Therefore, unveiling and synthesizing novel 2D ferromagnetic crystals with high T_C is still a great challenge.

A simple and straightforward way to attain monolayer or few-layer materials is to micromechanically exfoliate the bulk materials with layered phase. Recently, using high-

throughput first-principles calculations, Mounet *et al*.[24] examined 5619 experimentally known layered compounds and found that 1825 compounds are easily or potentially exfoliable due to the weak interlayer Van der Waals (vdW) interaction. Among them, 36 ferromagnetic systems were identified, offering rich opportunities to synthesize 2D ferromagnets; however, their Curie temperatures were not reported. Here we performed comprehensive first-principles calculations to evaluate the long-range magnetic order and Curie temperatures of these recently predicted ferromagnets. After a systematic screening, five 2D compounds (LaCl, YCl, ScCl, $LaBr_2$, and CrSBr) have been identified as robust ferromagnets with $T_C > 200$ K. As the isoelectronic analogies of CrSBr, three unprecedented 2D ferromagnetic semiconductors (CrSI, CrSCl, CrSeBr) with enhanced superexchange interaction and high T_C up to 500 K have been designed. These results enrich the existing database of 2D intrinsic ferromagnets and provide experimentally accessible systems to realize monolayer ferromagnetic materials and 2D spintronic devices.

2. COMPUTATIONAL METHODS

First-principles calculations were carried out using spin-polarized density functional theory (DFT) with the Perdew-Burke-Ernzerhof (PBE) exchange-correlation functional within the generalized gradient approximation (GGA),[25] as implemented in the Vienna *Ab initio* Simulation Package (VASP).[26-27] The projected augmented wave (PAW) potential was used to describe the ion-electron interaction.[28-29] To account for the possible effect of strongly correlated electrons, we also performed GGA + U single-point-energy calculations using Coulomb interaction parameter

U (5 eV and 6 eV for ScCl; 5 eV for YCl; 5 eV and 7.5 eV for LaCl and $LaBr_2$; 4 eV for Cr), and the exchange interaction parameters J (1 eV for all transition metals), respectively. These parameters have been well tested in previous studies.[30-32] The Grimme's DFT-D3 scheme was adopted to describe the interlayer long-range vdW interactions.[33] The energy cutoff of the plane-wave basis was 500 eV. During geometry optimization, numerical convergence was achieved with the tolerance of 10^{-5} eV in energy and 0.01 eV $Å^{-1}$ in force, respectively. To avoid the interaction between a layer and its replica, a vacuum space of 20 Å thickness was added. The 2D Brillouin zone was sampled by Monkhorst-Pack **k**-point grid with a uniform spacing of 0.01 $Å^{-1}$. Our PBE calculations with Grimme's D3 dispersion correction can reasonably reproduce the experimental lattice parameters of the five known compounds with layered bulk phase (see Table S1).

For the hypothetical monolayer structures, their phonon dispersions were computed using the direct supercell method as implemented in the Phonopy program.[34] *Ab initio* molecular dynamics (AIMD) simulations were also performed to assess the thermal stabilities. The thermodynamic stability of all these monolayer compounds were evaluated by the heat of formation (H_f), which is defined by $H_f = xE_A + yE_B + zE_C - E_{A_xB_yC_z}$, where $E_{A_xB_yC_z}$ stands for the energy of $A_xB_yC_z$ compound, E_A, E_B, and E_C is the energy per atom of A, B and C elements in their most stable solid or gas phase, respectively. By definition, a positive H_f means formation of the compound is exothermic. To assess the possibility of mechanically exfoliating the layered bulk crystal, we computed the interlayer binding energy E_B defined as $E_B = \left(E_{monolayer} - E_{bulk}/m\right)/n$, where $E_{monolayer}$ and E_{bulk} are the total energy of the monolayer and bulk phases, respectively, m is the

number of layers per unit cell in bulk crystal, *n* is the number of atoms per monolayer.

We evaluated the Curie temperature of these 2D ferromagnets by both mean-field theory (MFT)[35] and Monte Carlo (MC) simulations based on Ising model. Here we consider nearest and next-nearest neighboring coupling of on-site spin (*M*), the Hamiltonian can be written as $H = -\sum_{i,j} J_1 M_i M_j - \sum_{k,l} J_2 M_k M_l$, where the exchange coupling parameters J_1 and J_2 are extracted from the energy differences of ferromagnetic (FM) and antiferromagnetic (AFM) states. For every monolayer compound, MC simulations of 1.2×10^5 iterations at each temperature were carried out on a 120×120 lattice, which has been carefully assessed to be big enough for MC simulations.

3. RESULTS AND DISCUSSION

To avoid the possible computational difficulty with rare earth elements by DFT, here we investigated 22 non-rare earth compounds from the 36 potential 2D ferromagnets predicted by Mounet *et al*.[24] Their magnetic properties including T_C from mean-field theory (MFT) simulations based on our DFT calculations are described in Table S2. Among 22 systems considered, five novel 2D compounds (LaCl, YCl, ScCl, $LaBr_2$, and CrSBr) have been identified as robust ferromagnets with relatively high T_C (> 200 K). According to the space group, the five monolayer structures can be divided into three types: type *i* (LaCl, YCl, ScCl), type *ii* ($LaBr_2$), and type *iii* (CrSBr) belonging to $P\bar{3}M1$, $P\bar{6}M2$, $PMMN$, respectively. Their atomic structures are depicted in Figure 1; the lattice parameters and fractional coordinates are listed in Table S3. In all

these monolayer structures, the transition metal (TM) atoms are hexa-coordinated. The type *i* and *iii* structures have two layers of TM atoms, while type *ii* has only one layer of TM atoms. Especially, type *iii* has an orthorhombic structure, in which each Cr ion is coordinated by four chalcogenide and two halide ions, leading to a distorted octahedron (see Figure 3a).

The spin-polarized band structures of these five 2D compounds are displayed in Figure 2. The compounds of type *i* (LaCl, YCl, ScCl) are metal, in agreement with the previous finding.[24] The metallicity stems mainly from the *d* orbitals of TM atom. Meanwhile, monolayer compounds of both type *ii* and type *iii* are semiconductors with small bandgap (E_g = 0.62 eV for $LaBr_2$, E_g = 0.23 eV for CrSBr) from PBE calculations. As revealed by the partial density of states (PDOS) in Figure S1, the valence band maximum (VBM) and conduction band minimum (CBM) of monolayer $LaBr_2$ are dominated by the $d_{x^2-y^2}$ and d_{xy} orbitals of La atoms, whereas the d_{z^2} orbital contributes to CBM as well. The CBM and VBM of monolayer CrSBr are primarily contributed by the spin-up states of the Cr-d_{z^2} and Cr-d_{xz} orbitals with large spin splitting.

Figure S2 presents the spin density distributions of LaCl, $LaBr_2$, and CrSBr in their stable FM configurations, showing that the magnetism is originated mainly from TM atoms. For LaCl and $LaBr_2$ compounds of type *i* and type *ii*, the spin density is relatively delocalized in the intermediate region between La atoms, resulting in a weak magnetic moment of ~0.4 μ_B per La atom. In contrast, monolayer CrSBr of type *iii* carries a sizeable magnetic moment of 3 μ_B per Cr atom with the spin density mainly localized on Cr atom, whereas S atoms are antiferromagnetically polarized with a small magnetic moment (–0.143 μ_B). The difference in the spin density

distributions of La and Cr atoms could be intuitively related to their electronegativities (1.10 for La and 1.66 for Cr in Pauling scale); in other words, the La atom with less electronegativity exhibits more delocalized spin density distribution.

As schematically illustrated in Figure 3a-b, the origin of a large integral spin moment on Cr atom can be well interpreted by the distorted octahedral coordination. Due to symmetry breaking under octahedral crystal field, five degenerate *d* orbitals of Cr atom are split into e_g level (d_{z^2} and d_{xy}) with higher energy and t_{2g} level ($d_{x^2-y^2}$, d_{yz} , and d_{xz})with lower energy under current axis definition. In the monolayer CrSBr structure, distortion of octahedron leads to further splitting of e_g and t_{2g} levels; consequently, the five *d* orbitals are no longer degenerate. According to the atomic formal charge, each S atom should gain two electrons and each Br atom gain one electron from Cr atom ($[Ar]3d^5 4s^1$), respectively. Such trend of charge transfer from Cr to S and Br atoms can be qualitatively seen in the differential charge density in Figure 3c. Following Hund's rule, the three low-lying t_{2g} orbitals are singly occupied by the remaining three valence electrons on Cr atom with parallel spin, resulting in a net spin moment of 3 μ_B. This picture is further supported by PDOS of CrSBr in Figure 3d. The d_{xy}, d_{yz}, and d_{xz} orbitals in the spin-up states are occupied about 1 eV below the Fermi level, whereas all five *d* orbitals on the spin-down side are unoccupied.

For each 2D compound, we constructed various supercells with either FM or AFM ordering of the on-site spin, as illustrated in Figure 4. Their exchange energies ($E_{ex} = E_{AFM} - E_{FM}$) and magnetic moments from PBE calculations are summarized in Table 1, while the corresponding GGA + U results are given in Table S4. In line with previous PBE calculations,[24] we find that all

these 2D systems prefer FM configuration as the magnetic ground state, mostly irrelevant to the inclusion of U term, except for LaCl monolayer with U_{eff} = 6.5 eV. The on-site magnetic moments of transition metal atoms in these ferromagnetic 2D compounds from MC simulations are plotted as a function of temperature in Figure 5a. The resulting T_C values for these 2D compounds are given in Table 1, along with a diagram of T_C^{MC} in Figure 5b. Generally speaking, T_C values from MFT and MC show a consistent trend. For type *i* and *ii*, T_C^{MC} usually lie between the upper and lower bounds by MFT estimation. For type *iii*, however, MFT overestimates T_C by about twice with regard to MC simulation, which is a known deficiency of MFT. Nevertheless, the MC predicted Curie temperatures of all five systems (280 K for ScCl, 240 K for YCl, 260 K for LaCl, 280 K for $LaBr_2$, 290 K for CrSBr) are comparable to room temperature (300 K). Compared to recent reports, our T_C value is higher for ScCl (T_C = 185K[36]) and lower for LaCl (T_C = 400 K[37]), respectively, due to the usage of different theoretical models.

Among the current three types of 2D ferromagnetic structures, monolayer CrSBr of type *iii* stands out for its large magnetic moment and high T_C simultaneously. Its robust ferromagnetism is governed mainly by two superexchange interactions, as schematically illustrated in Figure 6e. The first one is the halogen-mediated (Cr-Br-Cr) and the chalcogen-mediated (Cr-S-Cr) superexchange interactions with the nearest Cr-Cr distance of 3.541 Å, and the second one is two chalcogen-mediated (Cr-S-Cr) with the next nearest Cr-Cr distance of 3.608 Å. According to the Goodenough-Kanamori-Anderson (GKA) rule, superexchange interaction is simultaneously determined by the symmetry of the crystal field, *d* electron configuration of the TM atom, orbital

hybridization between metal (M) and nonmetal (NM) atoms, and M-NM-M bond angles.[38] Since only three unpaired electrons are singly occupied on the 3*d* orbitals of Cr cation, hybridization from the *p* orbitals of S or Br tends to induce a parallel spin on the neighboring Cr cation. Moreover, the Cr-NM-Cr angles of about 90° (see Table S5) indicate that the Cr *d* orbitals couple with the orthogonal *p* orbitals from Br or S atom, e.g., Cr- $d_{x^2-y^2}$ with Br-p_x and S-p_x, Cr-d_{yz} with Br-p_z and S-p_x, respectively (see Figure S4 for PDOS analysis). In this case, superexchange is mediated via the Coulomb exchange on the orthogonally bonded S or Br atoms; thus the M-M magnetic coupling is expected to be ferromagnetic [5,39,40]. The positive exchange coupling parameters J_1 and J_2 in Table 1 and Table S4 also confirm that the first and second nearest superexchange interactions in CrSBr favor the stable FM state.

Based on the above analysis, we propose an effective strategy to tailor the superexchange coupling strength of 2D ferromagnets by isoelectronic substitution, meanwhile retaining the large on-site moment of Cr atom. By substituting Br with Cl/I or substituting S with Se/Te, we design four hypothetical monolayer structures of CrSCl, CrSI, CrSeBr, and CrTeBr that are both isoelectronic and isostructural to the CrSBr monolayer. Except for CrTeBr, the rest three structures are dynamically stable without imaginary frequency, as evidenced by the computed phonon dispersions in Figure S3a. Our AIMD simulations of CrSCl, CrSI, and CrSeBr also indicate that all of them are thermal stable at room temperature (300 K) after 10 ps (Figure S3b). Moreover, as shown in Table 1, the positive formation energies of these three hypothetical monolayer compounds are comparable to their mother structure CrSBr that has layered crystal in reality,

suggesting that 2D compounds of CrSI, CrSCl, and CrSeBr could be synthesized in bulk phase. From our PBE calculations, CrSBr, CrSCl, and CrSeBr are semiconductors with small direct bandgaps of 0.05~0.23 eV, while CrSI is an indirect semiconductor with E_g = 0.18 eV.

After isoelectronic substitution of the halogen and/or chalcogen atoms, the valence state of Cr^{3+} in these 2D compounds is unchanged, which in turn effectively retains the large on-site magnetic moment of 3 μ_B on Cr atom (see Table 1). However, isoelectronic substitution leads to different degrees of distortion of the octahedral crystal field on Cr atom (see Figure 3a), which can be seen in the variations of Cr-halogen and Cr-chalcogen bond lengths (l_1, l_2 and l_3) and characteristic bond angles (θ_1, θ_2, and θ_3) listed in Table S5. Such geometry changes, along with the variations in intrinsic electronic properties of the halogen and/or chalcogen atoms (e.g. electronegativity and atomic radius as listed in Table S6), lead to modification in the Cr-halogen and Cr-chalcogen bonding strengths, as revealed by the electron density counter plot in Figure 6. In this manner, the superexchange interaction between Cr cations via bridging the non-magnetic *p* orbitals of NM atoms is effectively modulated. Consequently, as shown in Figure 5, our MC simulations using exchange coupling parameters extracted from PBE calculations yield high T_C well above room temperature, i.e., 500 K for CrSCl and CrSeBr, demonstrating that isoelectronic substitution is able to significantly enhance the Curie temperature of 2D ferromagnetic compounds of type *iii*. In addition, the results of GGA + U calculations are given in Table S4. With inclusion of the possible electron correlation effect, the FM states in all eight 2D compounds remain robust. Especially, the Curie temperatures of the four semiconducting systems of type *iii* (290 ~ 350 K)

are still higher than or comparable to room temperature.

Finally, we assess the possibility of mechanical exfoliating the bulk crystals into monolayers in terms of the interlayer binding energies. As listed in Table 1, E_B lies in the range of 0.23 ~ 0.41 eV/atom, which is of the same order of magnitude as those of easily exfoliable TMD materials, e.g. E_B = 0.17 and 0.19 eV/atom for MoS_2 and $MoSe_2$ calculated using the same definition, respectively. Therefore, all these monolayer compounds, including the five systems with layered bulk phase in reality and the three hypothetical ones from our theoretical design, should be possibly exfoliated from their bulk materials.

4. CONCLUSION

In summary, among 22 easily or potentially exfoliable compounds with layered bulk structures, we screen out five intrinsically ferromagnetic 2D compounds (T_C > 200 K) and divide them into three structural types: type *i* (LaCl, YCl, ScCl) as metals, type *ii* ($LaBr_2$) and type *iii* (CrSBr) as indirect semiconductors. In particular, ferromagnetic monolayers of type *iii* possesses a large magnetic moment of ~3 μ_B on each Cr atom originated from its distorted octahedron coordination. The robust ferromagnetism in CrSBr monolayer is ascribed to the halogen-mediated (Cr-Br-Cr) and the chalcogen-mediated (Cr-S-Cr) superexchange interactions, which offer an isoelectronic substitution strategy to further tailor the magnetic coupling strength. Hence, monolayer structures of CrSI, CrSCl, and CrSeBr with notably enhanced Curie temperature up to 500 K are designed. The high T_C and feasibility for micromechanical exfoliation from their bulk

crystals (interlayer binding energy of 0.23 ~ 0.41 eV/atom) render the above-proposed monolayer materials credible candidates for 2D ferromagnetic materials and spintronic devices.

ASSOCIATED CONTENT

Supporting Information.

Magnetic properties including magnetic moment, exchange coupling parameter and Curie temperature (T_C), GGA + U results, lattice parameters, bond lengths and angles, atomic radiuses and electronegativities, spin-polarized partial density of states (PDOS), spin charge distributions, phonon dispersions and ab initio molecular dynamics (AIMD) simulation results, etc.

CORRESPONDING AUTHORS

* jiangx@dlut.edu.cn (Xue Jiang), zhaojj@dlut.edu.cn (Jijun Zhao)

ACKNOWLEDGMENTS

This work is supported by the National Natural Science Foundation of China (11574040, 11874097), the Xinghai Scholar project of Dalian University of Technology, and the project of Dalian Youth Science and Technology Star (2017RQ012). We also acknowledge the Supercomputing Center of Dalian University of Technology for providing the computing resource.

NOTES

The authors declare no competing financial interest.

REFERENCES

(1) Han, W. Perspectives for Spintronics in 2D Materials. *APL Mater.* **2016**, *4*, 032401.

(2) Li, X.; Wu, X. Two-Dimensional Monolayer Designs for Spintronics Applications. *Wires Comput. Mol. Sci.* **2016**, *6*, 441-455.

(3) Feng, Y. P.; Shen, L.; Yang, M.; Wang, A.; Zeng, M.; Wu, Q.; Chintalapati, S.; Chang, C. R. Prospects of Spintronics Based on 2D Materials. *Wires Comput. Mol. Sci.* **2017**, *7*, e1313.

(4) Liu, J.; Sun, Q.; Kawazoe, Y.; Jena, P. Exfoliating Biocompatible Ferromagnetic Cr-Trihalide Monolayers. *Phys. Chem. Chem. Phys.* **2016**, *18*, 8777-8784.

(5) Kulish, V. V.; Huang, W. Single-layer Metal Halides MX_2 (X = Cl, Br, I): Stability and Tunable Magnetism from First Principles and Monte Carlo Simulations. *J. Mater. Chem. C* **2017**, *5*, 8734-8741.

(6) Sivadas, N.; Daniels, M. W.; Swendsen, R. H.; Okamoto, S.; Xiao, D. Magnetic Ground State of Semiconducting Transition-metal Trichalcogenide Monolayers. *Phys. Rev. B* **2015**, *91*, 235425.

(7) Yu, M.; Liu, X.; Guo, W. Novel Two-Dimensional Ferromagnetic Semiconductors: Ga-based Transition-Metal Trichalcogenide Monolayers. *Phys. Chem. Chem. Phys.* **2018**, *20*, 6374-6382.

(8) Kan, M.; Adhikari, S.; Sun, Q. Ferromagnetism in MnX_2 (X = S, Se) Monolayers. *Phys. Chem. Chem. Phys.* **2014**, *16*, 4990-4994.

(9) Sun, Z.; Lv, H.; Zhuo, Z.; Jalil, A.; Zhang, W.; Wu, X.; Yang, J. A New Phase of the Two-Dimensional ReS_2 Sheet with Tunable Magnetism. *J. Mater. Chem. C* **2018**, *6*, 1248-1254.

(10) Zhao, T.; Zhou, J.; Wang, Q.; Kawazoe, Y.; Jena, P. Ferromagnetic and Half-Metallic FeC_2 Monolayer Containing C_2 Dimers. *ACS Appl. Mater. Interfaces* **2016**, *8*, 26207-26212.

(11) Wu, F.; Huang, C.; Wu, H.; Lee, C.; Deng, K.; Kan, E.; Jena, P. Atomically Thin Transition-Metal Dinitrides: High-temperature Ferromagnetism and Half-Metallicity. *Nano Lett.* **2015**, *15*, 8277-8281.

(12) Liu, Z. F.; Liu, J. Y.; Zhao, J. J. YN_2 monolayer: Novel p-State Dirac Half Metal for Highspeed Spintronics. *Nano Res.* **2017**, *10*, 1972-1979.

(13) Liu, J.; Liu, Z.; Song, T.; Cui, X.,Computational Search for Two-Dimensional Intrinsic Half-Metals in Transition-Metal Dinitrides. *J. Mater. Chem. C* **2017**, *5*, 727-732.

(14) Jiang, Z.; Wang, P.; Jiang, X.; Zhao, J. J. Mbene (MnB): A New Type of 2D Metallic Ferromagnet with High Curie Temperature. *Nanoscale Horiz.* **2018**, *3*, 335-341.

(15) Zhou, J.; Sun, Q. Magnetism of Phthalocyanine-Based Organometallic Single Porous Sheet. *J. Am. Chem. Soc.* **2011**, *133*, 15113-15119.

(16) Zhao, M.; Wang, A.; Zhang, X. Half-Metallicity of a Kagome Spin Lattice: The Case of a Manganese Bis-Dithiolene Monolayer. *Nanoscale* **2013**, *5*, 10404-10408.

(17) Liu, J.; Sun, Q. Enhanced Ferromagnetism in a $Mn_3C_{12}N_{12}H_{12}$ Sheet. *ChemPhysChem* **2015**, *16*, 614-620.

(18) Zhang, X.; Zhang, J.; Zhao, J.; Pan, B.; Kong, M.; Chen, J.; Xie, Y. Half-Metallic Ferromagnetism in Synthetic Co_9Se_8 Nanosheets with Atomic Thickness. *J. Am. Chem. Soc.* **2012**, *134*, 11908-11911.

(19) Xu, K.; Chen, P.; Li, X.; Wu, C.; Guo, Y.; Zhao, J.; Wu, X.; Xie, Y. Ultrathin Nanosheets of Vanadium Diselenide: A Metallic Two-Dimensional Material with Ferromagnetic Charge-Density-Wave Behavior. *Angew. Chem. Int. Ed. Engl.* **2013**, *52*, 10477-10481.

(20) Cheng, W.; He, J.; Yao, T.; Sun, Z.; Jiang, Y.; Liu, Q.; Jiang, S.; Hu, F.; Xie, Z.; He, B.; Yan, W.; Wei, S. Half-Unit-Cell Alpha-Fe_2O_3 Semiconductor Nanosheets with Intrinsic and Robust Ferromagnetism. *J. Am. Chem. Soc.* **2014**, *136*, 10393-10398.

(21) Xing, W.; Chen, Y.; Odenthal, P. M.; Zhang, X.; Yuan, W.; Su, T.; Song, Q.; Wang, T.; Zhong, J.; Jia, S.; Xie, X. C.; Li, Y.; Han, W. Electric Field Effect in Multilayer $Cr_2Ge_2Te_6$: A Ferromagnetic 2D Material. *2D Mater.* **2017**, *4*, 024009.

(22) Huang, B.; Clark, G.; Navarro-Moratalla, E.; Klein, D. R.; Cheng, R.; Seyler, K. L.; Zhong, D.; Schmidgall, E.; McGuire, M. A.; Cobden, D. H.; Yao, W.; Xiao, D.; Jarillo-Herrero, P.; Xu, X. Layer-Dependent Ferromagnetism in a Van Der Waals Crystal Down to the Monolayer Limit. *Nature* **2017**, *546*, 270-273.

(23) Gong, C.; Li, L.; Li, Z.; Ji, H.; Stern, A.; Xia, Y.; Cao, T.; Bao, W.; Wang, C.; Wang, Y.; Qiu,

Z. Q.; Cava, R. J.; Louie, S. G.; Xia, J.; Zhang, X. Discovery of Intrinsic Ferromagnetism in Two-Dimensional Van Der Waals Crystals. *Nature* **2017**, *546*, 265-269.

(24) Mounet, N.; Gibertini, M.; Schwaller, P.; Campi, D.; Merkys, A.; Marrazzo, A.; Sohier, T.; Castelli, I. E.; Cepellotti, A.; Pizzi, G.; Marzari, N. Two-Dimensional Materials from High-Throughput Computational Exfoliation of Experimentally Known Compounds. *Nat. Nanotechnol.* **2018**, *13*, 246-252.

(25) Perdew, J. P.; Burke, K.; Ernzerhof, M. Generalized Gradient Approximation Made Simple. *Phys. Rev. Lett.* **1996**, *77*, 3865-3868.

(26) Kresse, G.; Furthmuller, J. Efficient Iterative Schemes for *Ab Initio* Total-Energy Calculations Using a Plane-Wave Basis Set. *Phys. Rev. B* **1996**, *54*, 11169-11186.

(27) Kresse, G.; Furthmuller, J. Efficiency of *Ab-Initio* Total Energy Calculations for Metals and Semiconductors Using a Plane-Wave Basis Set. *Comp. Mater. Sci.* **1996**, *6*, 15-50.

(28) Blöchl, P. E. Projector Augmented-Wave Method. *Phys. Rev. B* **1994**, *50*, 17953-17979.

(29) Kresse, G.; Joubert, D. From Ultrasoft Pseudopotentials to the Projector Augmented-Wave Method. *Phys. Rev. B* **1999**, *59*, 1758-1775.

(30) Kanoun, M. B.; Goumri-Said, S.; Schwingenschlögl, U.; Manchon, A. Magnetism in Sc-Doped ZnO with Zinc Vacancies: A Hybrid Density Functional and GGA + U Approaches. *Chem. Phys. Lett.* **2012**, *532*, 96-99.

(31) Zhang, R.; Zhao, J.; Yang, Y.; Lu, Z.; Shi, W. Understanding Electronic and Optical Properties of La And Mn Co-Doped Anatase TiO_2. *Comp. Condens. Matter* **2016**, *6*, 5-17.

(32) Solovyev, I. V.; Dederichs, P. H.; Anisimov, V. I. Corrected Atomic Limit in the Local-Density Approximation and the Electronic Structure of dimpurities in Rb. *Phys. Rev. B* **1994**, *50*, 16861-16871.

(33) Grimme, S.; Antony, J.; Ehrlich, S.; Krieg, H. A Consistent and Accurate *Ab Initio* Parametrization of Density Functional Dispersion Correction (DFT-D) for the 94 Elements H-Pu. *J. Chem. Phys.* **2010**, *132*, 154104.

(34) Parlinski, K.; Li, Z. Q.; Kawazoe, Y. First-Principles Determination of the Soft Mode in Cubic

ZrO_2. *Phys. Rev. Lett.* **1997**, *78*, 4063-4066.

(35) Kittel, C. Introduction to Solid State Physics, 8th ed; *John Wiley & Sons*: Hoboken, NJ, **2005**, pp1323.

(36) Wang, B.; Wu, Q. S.; Zhang, Y. H.; Guo, Y. L.; Zhang, X. W.; Zhou, Q. H.; Dong, S.; Wang, J. L. High Curie-Temperature Intrinsic Ferromagnetism and Hole Doping-Induced Half-Metallicity in Two-Dimensional Scandium Chlorine Monolayer. *Nanoscale Horiz.*, **2018**, *3*, 551-555.

(37) Wu, M. H. High-Temperature Intrinsic Quantum Anomalous Hall Effect in Rare Earth Monohalide. *2D Mater*. **2017**, *4*, 021014.

(38) Stöhr, J.; Siegmann, H. C. Magnetism: From Fundamentals to Nanoscale Dynamics; *Springer-Verlag*: New York, **2006**, pp 274-276.

(39) Cai, B.; Chen, X.; Xie, M.; Zhang, S.; Liu, X.; Yang, J.; Zhou, W.; Guo, S.; Zeng, H. A Class of Pb-Free Double Perovskite Halide Semiconductors with Intrinsic Ferromagnetism, Large Spin Splitting and High Curie Temperature. *Mater. Horiz.* **2018**, *5*, 961-968.

(40) Huang, C. X.; Feng, J. S.; Wu, F.; Ahmed, D.; Huang, B.; Xiang, H. J.; Deng, K. M.; Kan, E. Toward Intrinsic Room-Temperature Ferromagnetism In Two-Dimensional Semiconductors. *J. Am. Chem. Soc.* **2018**, *140*, 11519-11525.

Table 1. Formation energy (H_f), interlayer binding energy (E_B), band gap (E_g), on-site magnetic moments (M) with TM for transition metal, Hal for halogen, Chal for chalcogen, energy difference (ΔE) between AFM state and FM state per unit cell, exchange coupling parameters (J_1, J_2) and Curie temperature (T_C^{MFT} stands for using mean-field theory, T_C^{MC} means using Monte Carlo simulations).

System	H_f/eV	E_B/eV	E_g^{PBE}/eV	M_{TM}/μ_B	M_{hal}/μ_B	M_{chal}/μ_B	ΔE/meV	J_1/meV	J_2/meV	T_C^{MFT}/K	T_C^{MC}/K
ScCl	1.45	0.36	0.00	0.447	0.002	-	52.10	8.71	2.16	0~453	280
YCl	1.51	0.35	0.00	0.450	0.007	-	2.45	0.40	4.95	0~358	240
LaCl	1.11	0.37	0.00	0.333	0.012	-	0.95	0.20	5.60	0~360	260
$LaBr_2$	1.62	0.41	0.62	0.403	0.007	-	25.33	6.38	-	0~444	270
CrSBr	0.80	0.25	0.23	3.000	0.001	-0.143	93.45	1.74	0.86	401~641	290
CrSI	0.59	0.23	0.18	3.007	-0.021	-0.135	101.60	1.53	1.28	475~759	**330**
CrSCl	0.91	0.27	0.61	2.996	0.010	-0.146	128.60	1.01	2.58	714~1143	**500**
CrSeBr	0.71	0.26	0.05	3.074	-0.008	-0.179	139.00	1.31	2.37	701~1122	**500**

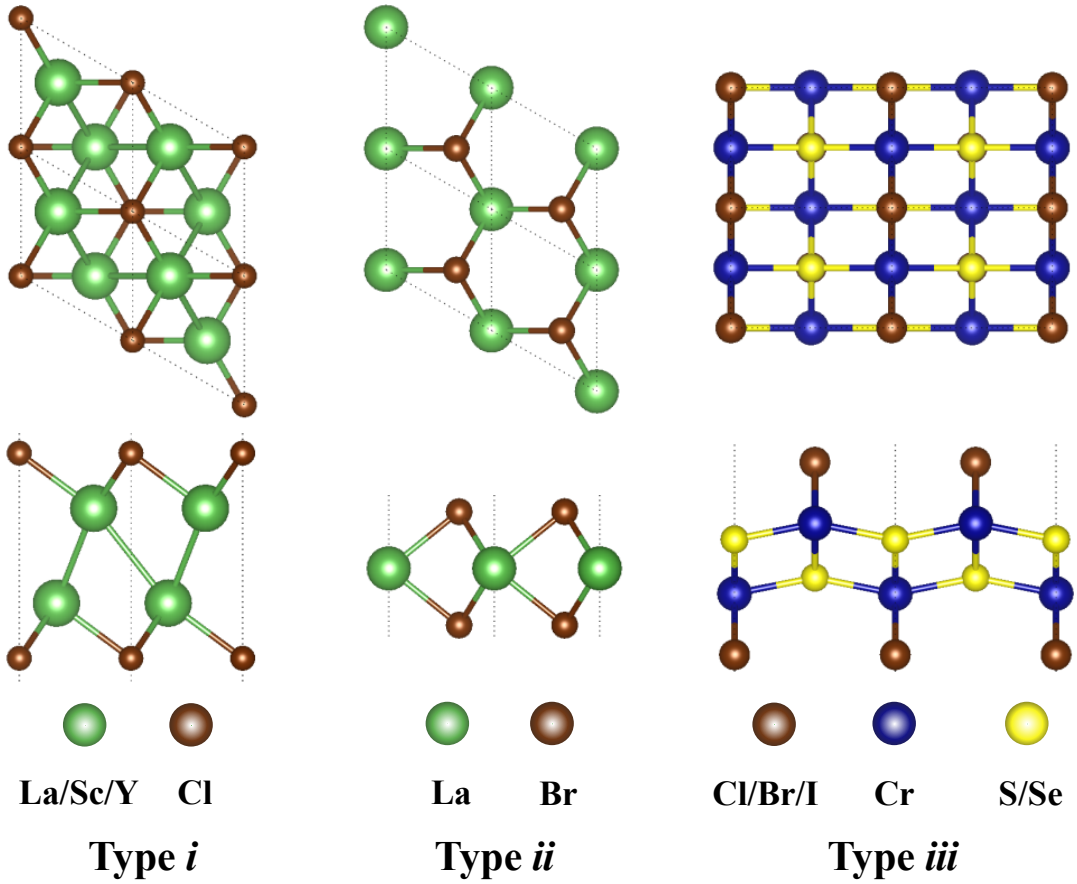

Figure 1. Atomic structures of three types of 2D monolayer compounds. The gray dotted lines represent the unit cell.

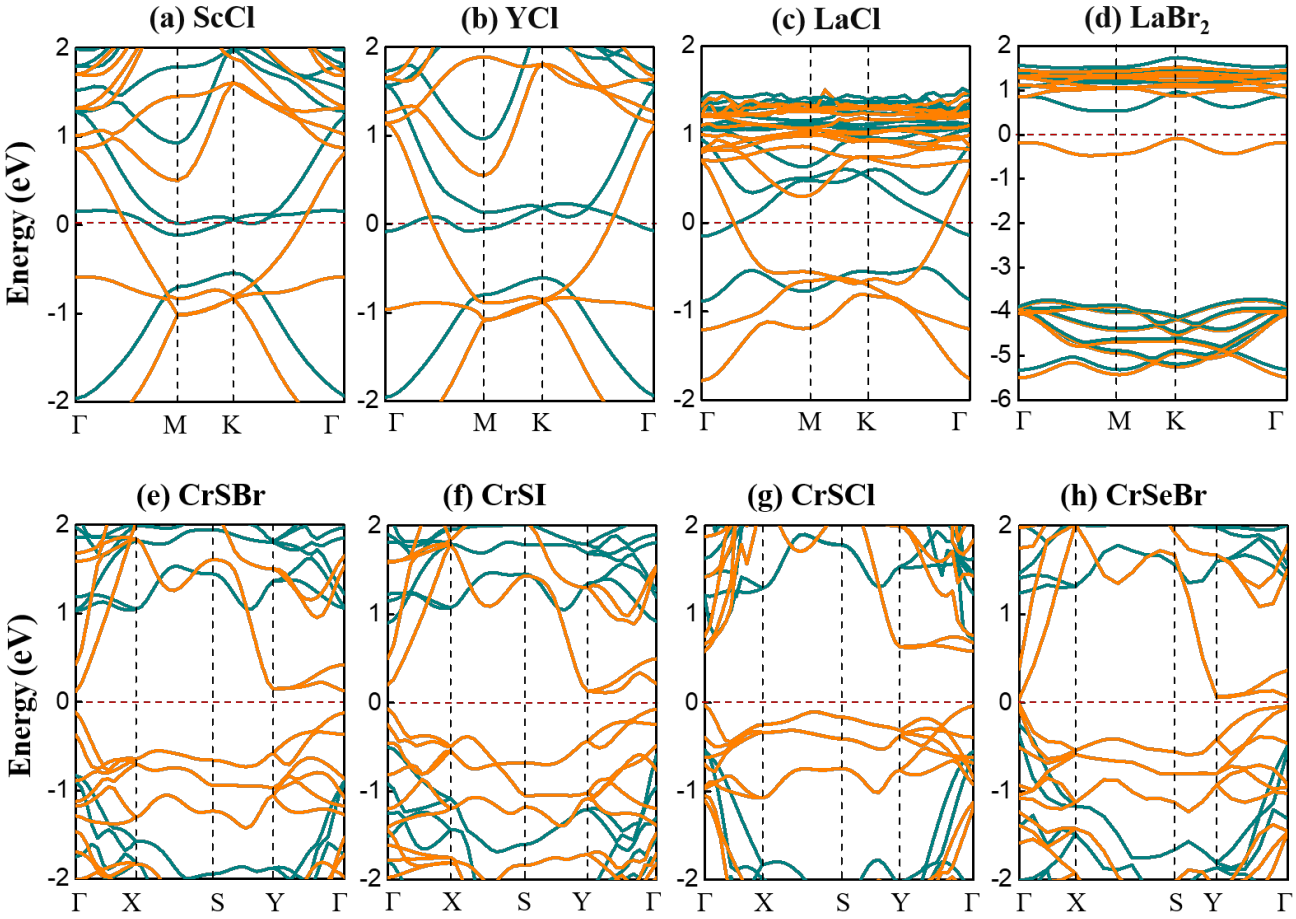

Figure 2. Spin-polarized band structures of 2D ferromagnetic compounds of type *i* : (a) ScCl, (b) YCl, (c) LaCl; type *ii*: (d) $LaBr_2$; type *iii*: (e) CrSBr, (f) CrSI, (g) CrSCl, (h) CrSeBr. Orange lines denote spin-up bands, and blue lines denote spin-down bands. Fermi level (red dashed line) is set to zero.

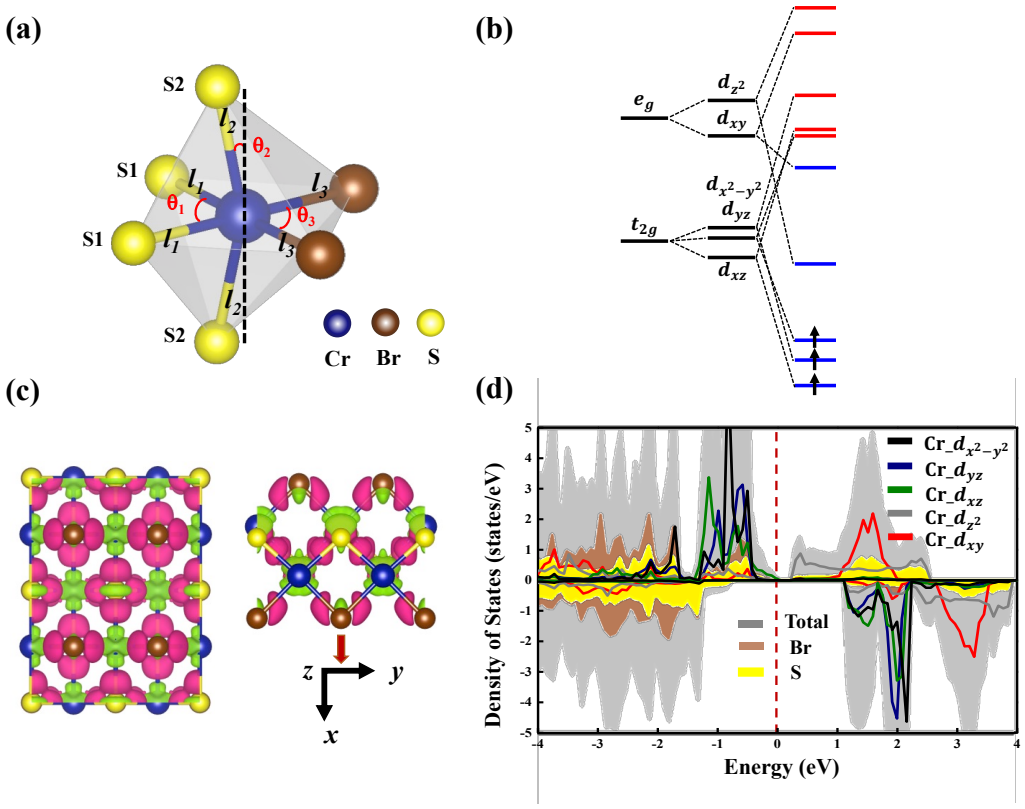

Figure 3. (a) Schematic structure of the distorted octahedron in CrSBr monolayer structure of type *iii*. The characteristic bond lengths (l_1, l_2, l_3) and angles (θ_1, θ_2, θ_3) are labeled. (b) Splitting of *d* orbitals of Cr atom under the octahedral crystal field of CrSBr monolayer. (c) Differential charge density (isovalue: 0.007 e/Å^3) of monolayer CrSBr. The dark pink and green color corresponds to charge accumulation and depletion, respectively. (d) Total (gray), atom-projected (brown for Br atom, yellow for S atom) and *d* orbitals evolved density of states on Cr atom for CrSBr monolayer, the Cr-4*s* state is not shown here since it is negligible within the considered energy range. The Fermi level (red dashed line) is set to zero.

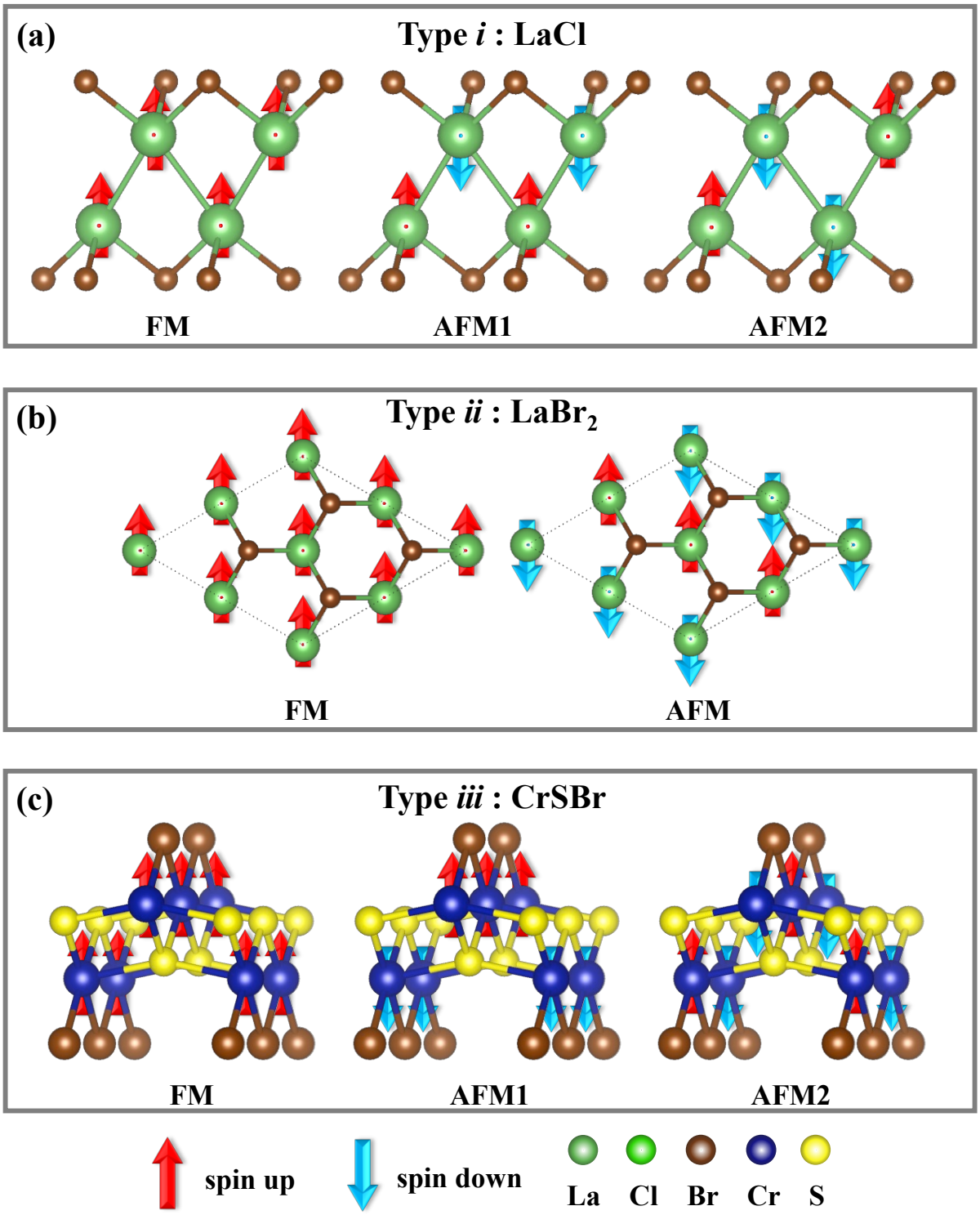

Figure 4. Schematic diagrams for (a) LaCl (type *i*), (b) $LaBr_2$ (type *ii*) and (c) CrSBr (type *iii*)

monolayers in FM and various AFM magnetic configurations. The red and blue arrows represent the magnetic atoms in spin-up and spin-down states, respectively.

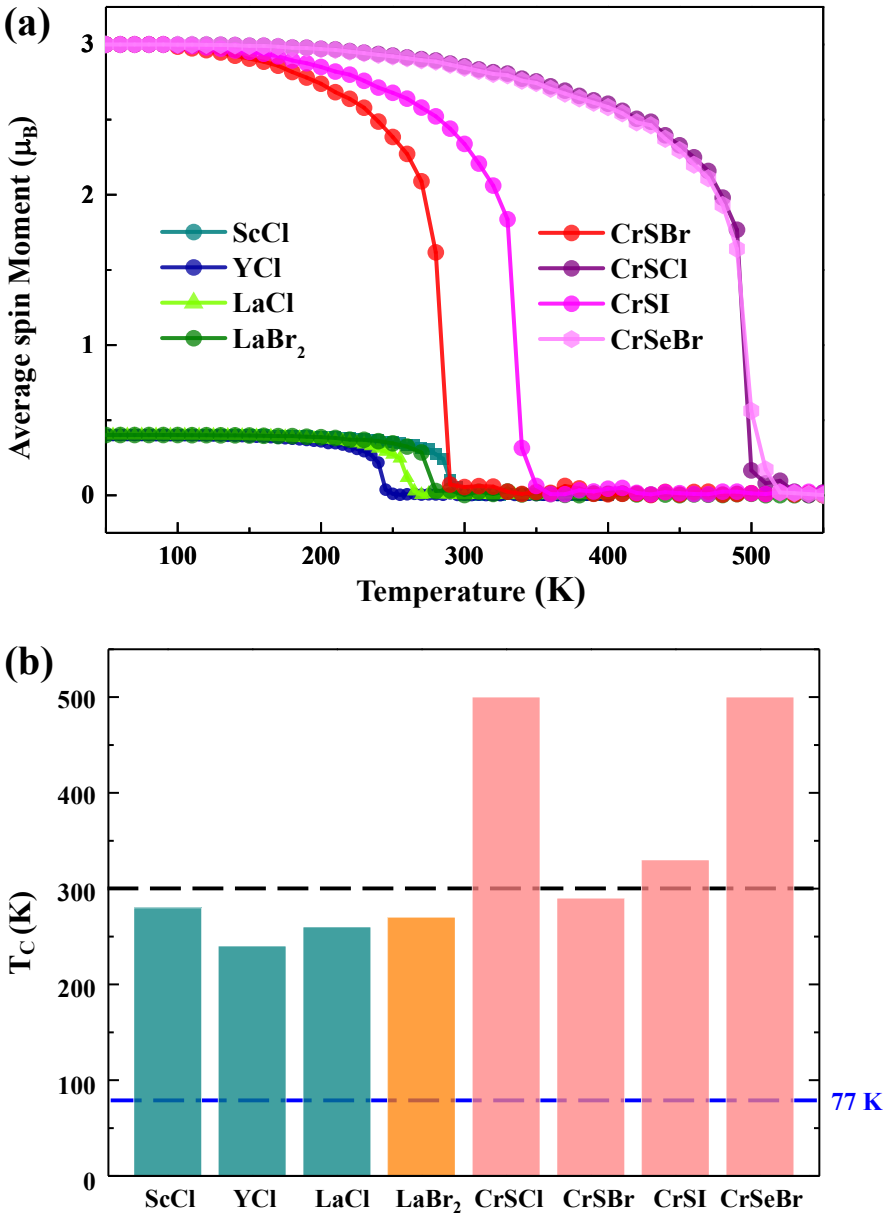

Figure 5. (a) On-site magnetic moments of transition metal atoms as a function of temperature in 2D ferromagnetic compounds with type *i* (YCl, ScCl, LaCl), type *ii* ($LaBr_2$), and type *iii* (CrSBr,

CrSCl, CrSI, CrSeBr) structures from MC simulations. (b) Curie temperatures of all eight 2D ferromagnets. The black and blue dotted lines represent the room temperature (300 K) and the liquid nitrogen temperature (77K), respectively.

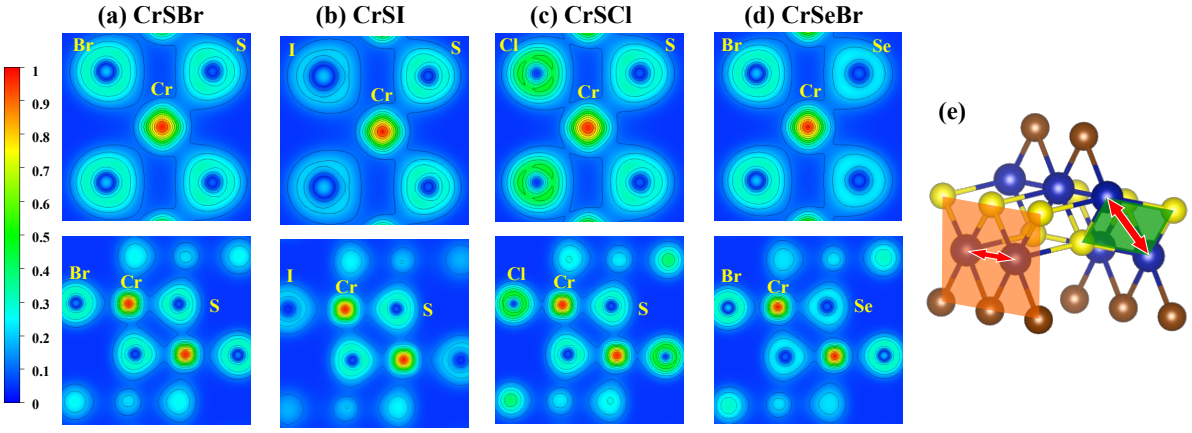

Figure 6. Contour plots for the electron densities of (a) CrSBr, (b) CrSI, (c) CrSCl, (d) CrSeBr monolayer structures. For each compound, the top and bottom panels pass through the orange and green slices in the 3D structural diagram shown in (e), respectively. Compared to CrSBr monolayer, the Cr-halogen bond is strengthened in CrSCl, and Cr-chalcogen bond is weakened in CrSeBr, respectively.

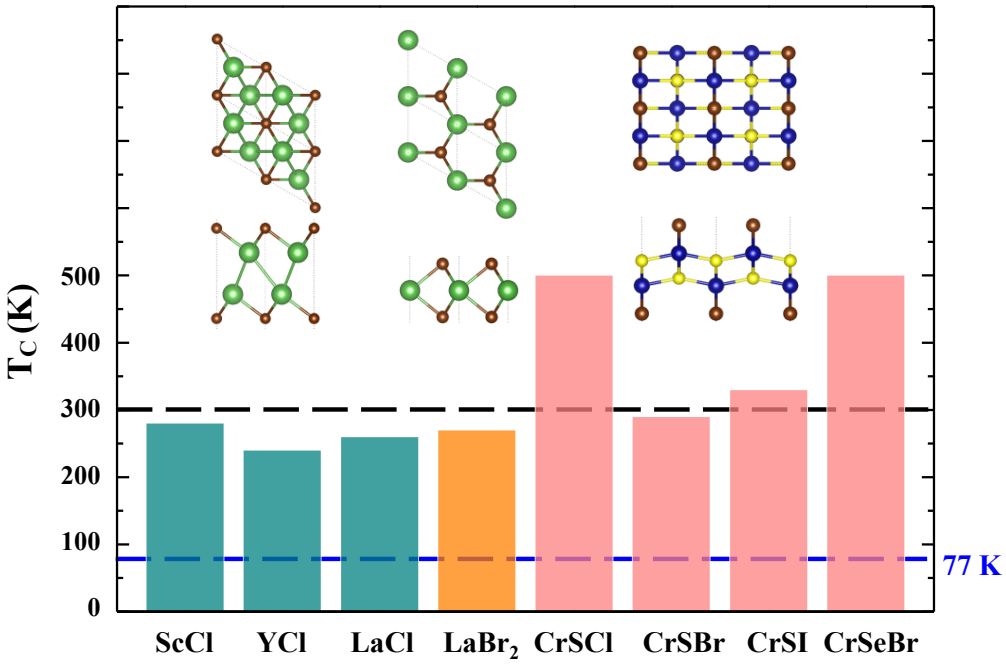

Graphical Abstract